

Article

Design of a Half-Bridge Current-Source Inverter Topology for Avionic Systems

Eralp Sener¹  and Gurhan Ertasgin^{2,*} 

¹ School of Mechatronics, Bilecik Seyh Edebali University, Bilecik 11230, Turkey; eralp.sener@bilecik.edu.tr

² School of Electrical & Electronic Engineering, Bilecik Seyh Edebali University, Bilecik 11230, Turkey

* Correspondence: gurhan.ertasgin@bilecik.edu.tr; Tel.: +90-228-214-17-07

Abstract: This paper analyses a new half-bridge current-source inverter for avionic systems. In the circuit, two 28 V batteries are used as inputs. These voltage sources are connected to inductors which create a constant current source. Then only two high-frequency switches are used to waveshape the positive and negative half-cycles. The SCR-based half-bridge allows positive and negative current flow properly. The inverter output uses a CL filter to remove PWM components and to obtain 400 Hz sinewave output. Simulation and HIL experiment results are provided with feedback control to prove the concept of the proposed topology. The study shows that the new current-source topology provides promising results while complying with aviation standards.

Keywords: current-source inverter; half-bridge; single-phase; energy storage inductor; aircraft



Citation: Sener, E.; Ertasgin, G. Design of a Half-Bridge Current-Source Inverter Topology for Avionic Systems. *Aerospace* **2022**, *9*, 354. <https://doi.org/10.3390/aerospace9070354>

Academic Editors: Peter Korba and Miroslav Kelemen

Received: 27 May 2022

Accepted: 25 June 2022

Published: 1 July 2022

Publisher's Note: MDPI stays neutral with regard to jurisdictional claims in published maps and institutional affiliations.



Copyright: © 2022 by the authors. Licensee MDPI, Basel, Switzerland. This article is an open access article distributed under the terms and conditions of the Creative Commons Attribution (CC BY) license (<https://creativecommons.org/licenses/by/4.0/>).

1. Introduction

More electric aircraft (MEA) is a critical solution to having more environmentally friendly and efficient aircraft. MEA replaces many functions traditionally driven by mechanical, pneumatic, and hydraulic power by electrical subsystems. The development of MEA has accelerated with the development of electrical machinery, power electronics and control techniques [1]. Power inverters are one of the electrical subsystems in aircraft. Inverters are designed in ground-type or plane-type. Static inverters have a 400 Hz output frequency [2–5]. Inverters with 400 Hz output frequency are also preferred for marine, rail transport and laboratory research for a long time [6]. Although voltage-source static inverters (VSI) are studied and designed for such applications [7,8] current-source inverters could not find a place in the literature [4].

This study is going to present a novel 400 Hz current-source half-bridge inverter (CSI) topology for avionics.

1.1. Theoretical Background

When aviation started using electricity, the form of electricity used was DC. As AC became more popular in aviation, the problem was the weights and dimensions of transformers, motors and power supplies. The idea of using a high frequency to make the components smaller was proposed [9]. The short transmission lines made the increased losses negligible. Reference is made to a United States Military Standard MIL-STD-704F for using 400 Hz voltage frequency in aircraft. Table 1 shows some of the standard parameters.

Transporting energy with high frequency has some drawbacks. The use of 400 Hz frequency at the output of the converters causes them to be more sensitive to voltage drops and the resulting losses are essentially reactive. The inductive behavior of the transmission lines causes reactive losses. Current frequency and conductor length cause the losses. Higher amplitude voltage drops can be seen if there is an increase in frequency compared to lower frequencies (50/60 Hz). Therefore, there is a critical trade-off between frequency and transmission lines. However, the total loss is much higher when higher volume

components are used with lower frequency. As a result, this trade-off still allows the losses to be ignored to have smaller sizes and weights.

Table 1. Operation Characteristics of 400 Hz AC [10].

Steady State Characteristics	Limits
Voltage	108.0 to 118.0 V, rms
Voltage Unbalance	3.0 V, rms max.
Voltage Modulation	2.5 V, rms max.
Voltage Phase Difference	116° to 124°
Distortion Factor	0.05 max.
Crest Factor	1.31 to 1.51
DC Component	+0.10 to –0.10 V
Frequency	393 to 407 Hz
Peak Voltage	±271.8 V

1.2. Current-Source Inverter

In current-source inverters, the input current is constant and the output current is independent of the load. The current supplied from the source is kept at a constant level regardless of the load or the conditions of the inverter. However, in voltage-source inverters widely used in industry, the input voltage is kept constant and the variable output voltage is independent of the load.

Current-source inverters are less preferred than voltage-source inverters as they use large inductors to avoid fluctuations at the DC link. This is because a double line frequency ripple (100/120 Hz or 2ω ripple) is inherent in single-phase DC/AC PWM converters. Current-source inverters must use a big inductor to regulate the power imbalance between the DC and AC sides whereas VSIs employ a big capacitor (see Figure 1a). These capacitors have significantly less volume compared to CSIs for the same energy storage capability. Figure 1b shows a block diagram of a current-source inverter with a bulky DC link inductor in series to enable a ripple-free current at the DC link.

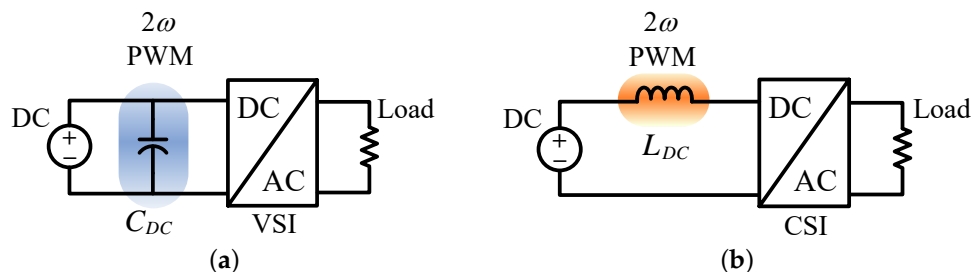


Figure 1. (a) Typical voltage-source inverter block diagram and (b) current-source inverter block diagram indicating input energy storage elements which reduce 2ω and PWM ripples.

For single-phase or three-phase inverters, the energy storage component at the DC link is a trade-off between the volume and power reduction [11]. This is very important for single-phase CSIs compared to three-phase inverters due to single-phase switching. Double line frequency fluctuations increase both rms and instantaneous current flow in the circuit. That, in turn, can lead to the use of higher power rating components and result in higher losses. This situation sometimes even causes saturation of the magnetic elements. Therefore, it is desired to design smaller energy storage elements and hence smaller systems. Considering the cost, size, weight and reliability (especially electrolytic capacitors), it is desirable to minimize the DC link energy storage. The minimum energy storage has two limits:

- The maximum acceptable input current or voltage ripple causing average power loss at the output of the DC supply.

- The maximum acceptable current ripple (for CSI) or voltage ripple (for VSI) at the input of the inverter causing distortion before an unacceptable level found in the output current of the inverter feeding a load.

The most popular way to separate these two limits is to use a two-stage VSI. This decoupling circuit is accomplished by adding a DC/DC converter before VSI as seen in Figure 2. This additional converter isolates the power supply at the DC input from 2ω fluctuations. The input capacitor (C_{IN}) only filters power variations caused by PWM switching. The DC link capacitor (C_{DC}) at the input of the inverter provides the necessary energy storage for 2ω fluctuations. However, the two-stage inverter has disadvantages such as decreased efficiency and increased cost [12].

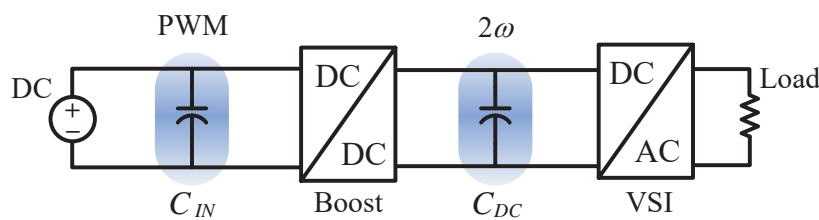


Figure 2. Two stage converter decoupling circuit.

Different approaches have been proposed to reduce the DC link energy storage element. These are classified as: (1) passive power decoupling with passive components and (2) active power decoupling circuits with the use of semiconductor switches.

A conventional current-source topology with a resonant filter at the DC link and a different modulation technique has been proposed [13]. This passive power decoupling technique reduces the ripples and provides 95% efficiency. Although the efficiency is quite high for a CSI, the double-tuned parallel resonant circuit increases the cost of the system with extra passive components. A four-switch three-port VSI is proposed with a passive power decoupling using a few passive components [14,15]. However, the inductors require optimization to increase efficiency to acceptable levels for VSIs such as 95%. A current-source inverter uses a decoupling technique based on DC/DC flyback converter without extra switches [16]. The energy storage inductor is not sufficient to reduce the current ripple to the maximum allowable input current level.

An active power decoupling circuit has been proposed for a VSI with some extra switches in the main current path [17]. Although the topology uses film capacitors to improve the lifetime of the system the complexity of the inverter is increased and the efficiency is reduced. Different modulation technique is used for a CSI to reduce the size of the DC link inductor [18,19] however it requires an extra analog circuitry to change the modulation function of the conventional sinusoidal PWM. The topology has high power reduction at the DC link as the fluctuations are substantially higher than the maximum allowable current fluctuations. A parallel active filter has been proposed to smooth 2ω ripples [20] in a CSI. This extra circuitry has passive components and switches to reduce the current ripple. As a result, there are more losses in the system and the overall efficiency of the system decreases [21]. Similarly, a CSI uses a power decoupling circuit with soft switching to reduce losses [22,23]. The number of current circulations increases therefore the circuit applications are limited and the system has more conduction losses.

Single-phase current-source inverters have a lower power-to-volume ratio compared to their voltage-sourced counterparts [24]. Therefore, they have more losses for the same power level compared to VSIs. This is valid for 50 or 60 Hz line frequency. Since 400 Hz output frequency is used in aviation, 800 Hz fluctuations occur instead of 100/120 Hz. Hence damping these fluctuations will require much smaller energy storage elements. In that case, current-source inverters will be advantageous. Consequently, CSIs can be used instead of voltage-source inverters in the avionics industry. The current-source inverter has several advantages over the voltage-source inverter, as follows [25,26]:

- They do not need a large capacitor at the DC link as it affects the lifetime and reliability of the inverter;
- No freewheeling diodes are required when operating into an inductive load, therefore the cost of the system is reduced;
- They can survive an output short circuit thereby allowing fault ride-through properties.
- CSIs can handle capacitive loads relatively easily, however, capacitive loads can cause large current spikes in a VSI;
- Power switches are highly utilized, unlike the VSIs, the current from the supply is switching between them, therefore the switches conduct for a full conducting cycle;
- CSIs have a higher output voltage than the input voltage. VSI topology is acting as a buck converter and it features an output voltage lower than the input voltage;
- The EMI generation is low compared to VSIs as changing currents generates EMI; however, CSIs have substantially constant current.

This paper aims to describe a new inverter topology. Batteries and DC link inductors create a constant current source in the DC link. Similar to a generic boost converter topology, there are high-frequency switches after the inductors. Sinusoidal pulse width modulation (SPWM) drives these switches. Thyristors that are switched with line frequency (400 Hz) come after high-frequency switches as a half-bridge. A low-pass filter completes the topology. Half-bridge inverters are suitable for use with wide bandgap semiconductors. A study compares SiC and GaN switch performances in a half-bridge inverter for a high switching frequency [27]. An induction heating application also used a voltage-source half-bridge inverter with a high switching frequency [28]. However, in the proposed current-source inverter topology, the half-bridge operates at 400 Hz using SCRs and takes advantage of the zero current switching feature. A wide-bandgap version of a MOSFET switch can be a good choice in the system as a high-frequency modulation switch before SCR based half-bridge. Using wide-bandgap switches is desirable for aerospace applications as they reduce the dimensions of the converter system and increase the switching frequency.

The layout of the paper is as follows: Section 1.3 describes the system, Section 1.4 describes the control scheme, Section 2 describes the simulation results of the system and Section 3 describes experimental results.

1.3. System Description

The proposed topology is inspired by a current-source single-phase inverter study [4]. However, the earlier topology includes an energy storage inductor at the DC link and a high-frequency MOSFET after the inductor. Figure 3 shows the new CSI topology that comprises two smaller inductors to produce a constant current source. MOSFET switches follow the inductors to shape the current with the SPWM. A half-bridge inverter unfolds the PWM modulated second half of the pulses before a capacitive-inductive (CL) low-pass filter to create a sinusoidal waveform. Please note that only two high-frequency switches modulate the waveform sinusoidally. Thyristors are preferred instead of MOSFETs. Therefore there is no need to employ series diodes with the MOSFETs.

The proposed CSI topology has some advantages:

- Reduced switching loss due to single switch modulation, which also leads to zero current switchings for thyristors;
- the current through the SCR drops below the value of the holding current naturally and prevents crossover distortion;
- low component count in the main current path. This topology does not include series diodes with SCRs to block reverse voltages. In addition, SCRs do not require any snubber circuit as they commutate naturally due to the waveshaper output current.

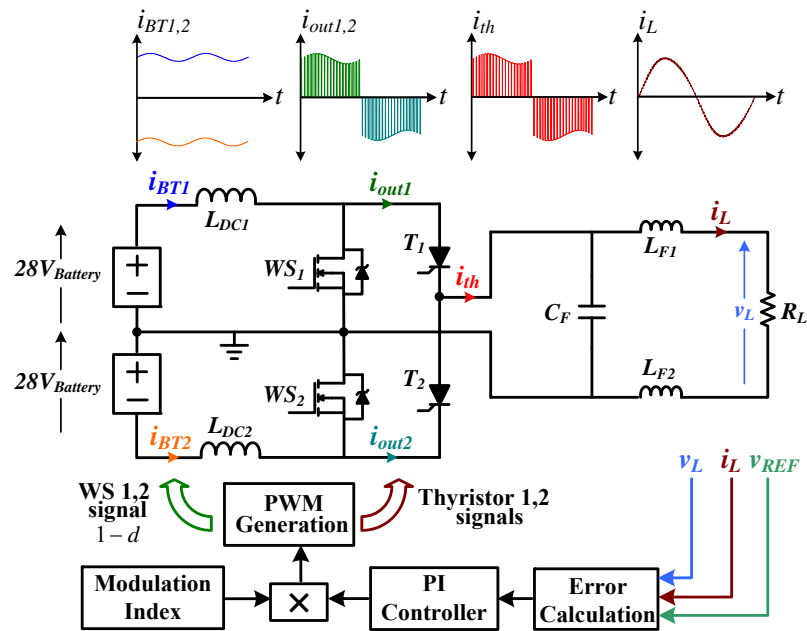


Figure 3. Current–source inverter circuit with control and current waveforms.

1.4. Control Scheme

Figure 4 depicts the principle operation modes of the proposed current–source inverter. For aviation applications, different design parameters are required compared to industrial applications. The aircraft industry considers size and weight as critical parameters. Therefore, a converter design with four semiconductor switches and two DC link inductors allows being small size and low weight whilst being robust and reliable.

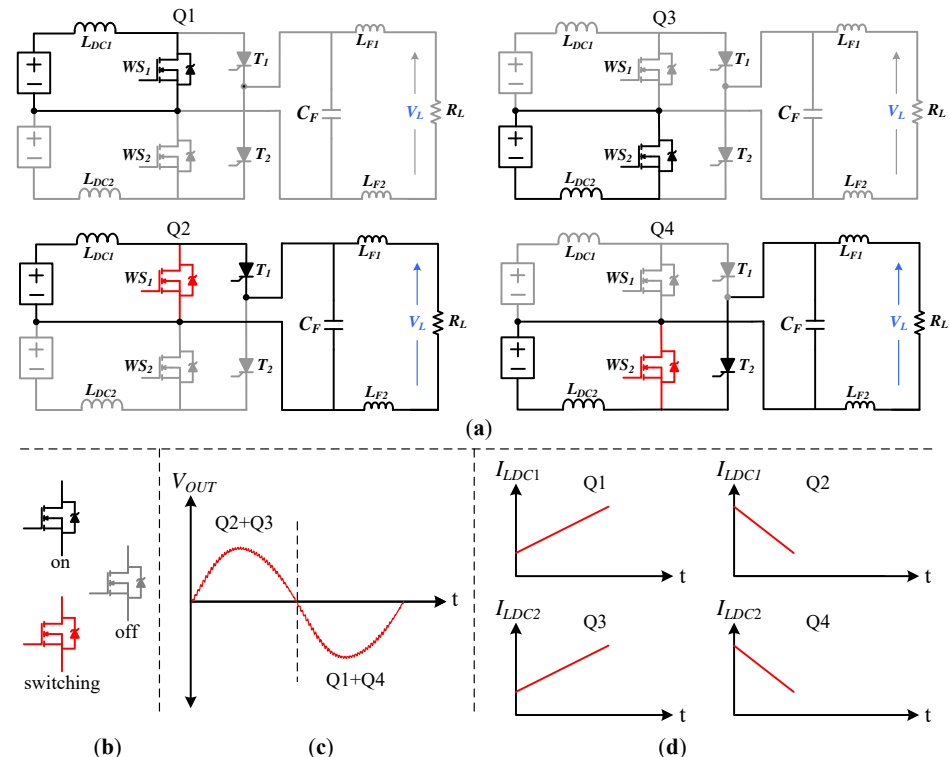


Figure 4. The switching states of the half-bridge CSI, (a) operation modes (b) conduction modes (c) V_{out} including operation modes and (d) current on the inductors L_1 and L_2 .

Two high-frequency switches shape the output waveforms. The upper MOSFET WS_1 modulates the positive half cycle of the generated sine waveform and the bottom one WS_2 modulates the negative half cycle of the waveform. Then both SCRs control the PWM chopped current flow to the output filter by switching at line frequency (400 Hz). After that, a CL output filter removes the high-frequency components to have a better sinusoidal output.

Open-loop analysis of the circuit is done using MATLAB Simulink. The obtained transfer function for open loop circuit is shown in (1).

$$\frac{1.092 \times 10^6 s + 1.229 \times 10^9}{s^2 + 1661s + 1996} \quad (1)$$

Figure 5 shows the bode diagram of the open-loop system to show the changes in magnitude and phase as a function of frequency. The control system designed for this system is based on a double loop PI control of which consists voltage and current feedback for stabilization.

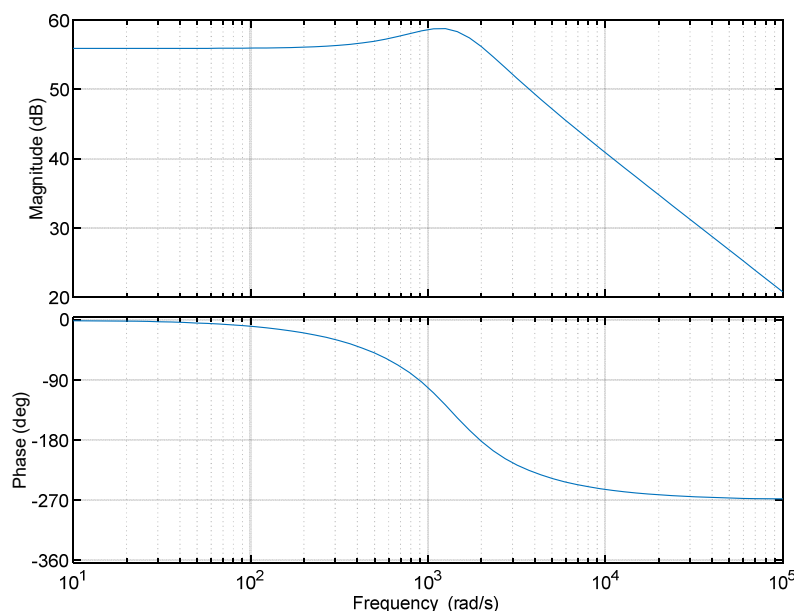


Figure 5. Gain plot (top) and phase plot (bottom) of the proposed CSI.

One of the most important characteristics of an aircraft power system is better power quality. There are many approaches to control inverters by using closed-loop control to obtain better current and voltage waveform. Various voltage control techniques have been developed to meet strict requirements. They are classified into two main techniques associated with the control structure single loop voltage control [29] and double loop voltage control [30].

Figure 6 shows the double loop control algorithm. A PI controller with current and voltage feedback has been added to the circuit. The RMS values of the output currents and voltages are taken to use a PI controller suitable for the DC system. Since this system is mainly a proof of concept, more complex control approaches have not been considered.

The required voltage $r(s)$ is given to the subtraction function as a unit function and the measured output voltage is divided by the required voltage and $y(s)$ is obtained for comparison with the unit function in the subtraction function. The error function $e(s)$ is determined due to the subtraction. After that, a PI controller is used to calculate the control signal $u(s)$. The load current variation as a feedback value is acquired from the current output. The resulting current value is subtracted from $u(s)$ to obtain a secondary feedback loop for a more stable system. The Ziegler–Nichols method is applied to determine the control parameters. This method starts by making the integral gain zero and then increasing

the proportional gain until the response oscillates. When the system oscillation has detected a value of K_p at the point of instability (K_{CR}) and critical frequency (f_{CR}) can be extracted. Table 2 shows the controller parameters obtained from the Ziegler–Nichols frequency response method. The gain constants K_p and K_i are obtained by using the determined K_{CR} and f_{CR} values in the table.

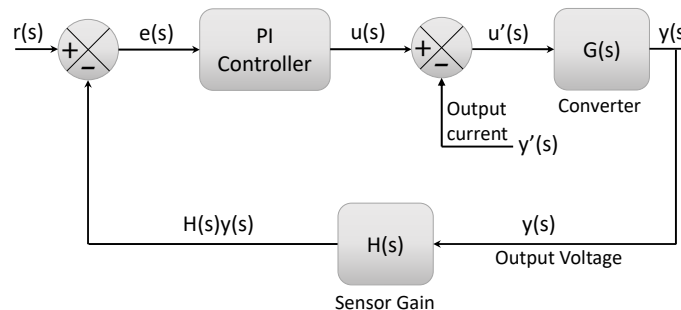


Figure 6. The closed-loop control block diagram of the proposed CSI.

Table 2. Ziegler–Nichols control parameters for P and I gains.

Controller Type	K_p	K_i
PI	$0.45 K_{CR}$	$1.2 f_{CR}$

The designed control system measures the output voltage and divides it by 115 (which can be any other reference voltage value) to obtain a unit signal. It is then subtracted from 1 to produce the error value. The resulting error value is connected to the PI controller. The current feedback signal multiplied by 0.01 is subtracted from the output of the PI controller. Then the obtained control signal is subtracted from 1 to produce an inverse control signal that can work with the CSI modulation technique. The final control signal is multiplied by a 400 Hz reference sine wave. The generated sinusoidal waveform is used as the modulation reference signal.

2. Inverter Simulations

2.1. Ideal Operation Test

The inverter was simulated using PSIM. The simulation circuit is shown in Figure 7. This circuit shows the concept of an inverter supplying AC. MOSFETs were used for modulation and thyristors were used for the output inverter half-bridge. The CSI does not have an output transformer considering transformers have an adverse effect in terms of efficiency. SCR voltage drops and passive element resistances were 1.2 V and 0.01Ω . A PI controller is used in the closed-loop control process.

Table 3 provides the simulation parameters of the inverter. 400 Hz CSI was designed considering the necessary conditions for aircraft. The parameters in the table agree with the requirements [10].

Table 3. Simulation parameters of the proposed half-bridge CSI topology.

Parameter	Value
Input Voltage	56 V
Input Current	26 A
Output Voltage	120 V rms
Output Current	12 A rms
Output Power	1.4 kW
DC link Inductors (L_{DC1}, L_{DC2})	5 mH
Filter Inductors (L_{F1}, L_{F2})	600 μ H
Filter Capacitor (C_F)	20 μ F
Switching Frequency	50 kHz

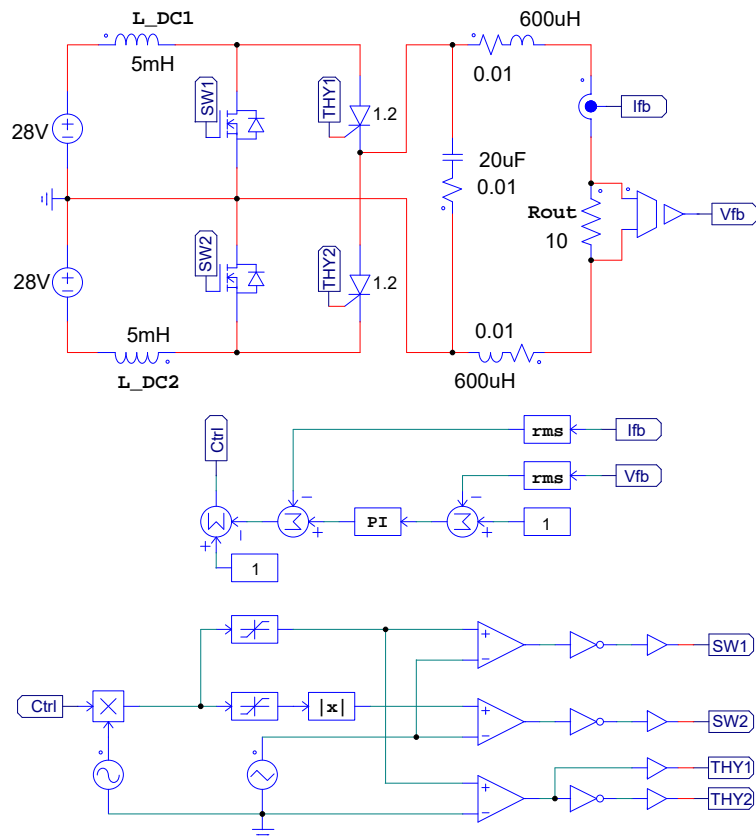


Figure 7. Proposed half-bridge CSI circuit simulation, showing current–source, waveshaper switches, half-bridge inverter and closed-loop control blocks.

Figure 8 shows the input and output waveforms of the CSI. Single-phase fluctuations of the output power cause DC link current and voltage fluctuations. There is a trade-off between the ripples on the current flowing through the DC link inductor and the inductance value. Figure 9 shows this trade-off for various ripple currents as a function of inductor values. In the simulations and HIL experiments, 5 mH inductors were used to be more on the small side. It can also be seen that the ripples are at the same frequency as the output power. The output current total harmonic distortion (THD) is 1.7%. It complies with the standards [31]. In addition, as can be seen from the output current and voltage waveforms, the power factor is almost unity [10].

Figure 9 shows the upper DC link inductor currents for different inductance values. As stated earlier, there is a trade-off between the inductance and ripple current magnitude. An increase in the inductor value results in a decrease in ripple current magnitude. Increasing inductor value reduces losses due to fluctuations however increases the inductor size and weight.

Please note that in a single-phase current–source inverter with 50/60 Hz output frequency, the DC link inductor will be significantly large compared to a current–source inverter with 400 Hz output frequency.

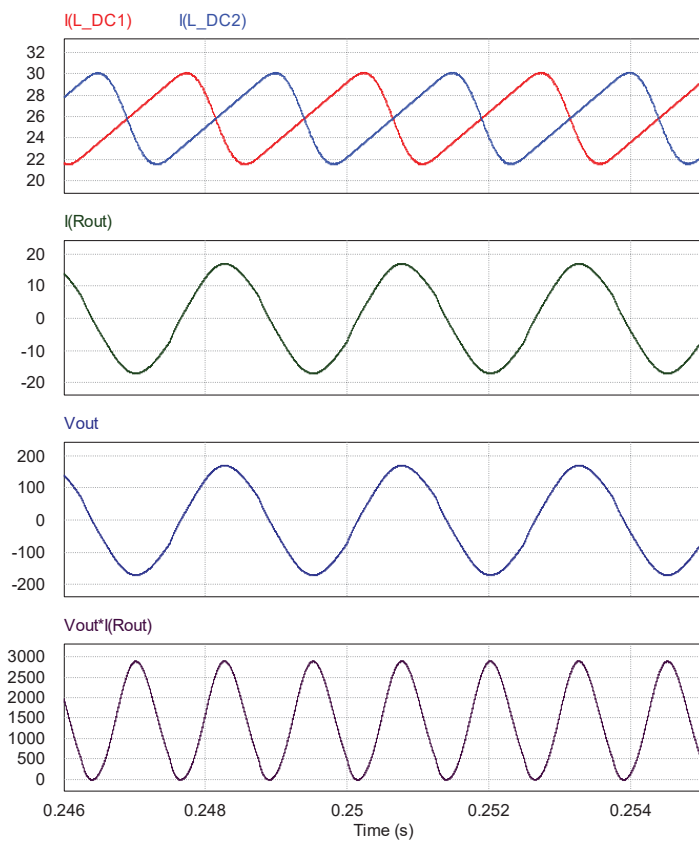


Figure 8. Simulation of the current at the DC link, output current and voltage of the inverter and inverter output power (top to bottom).

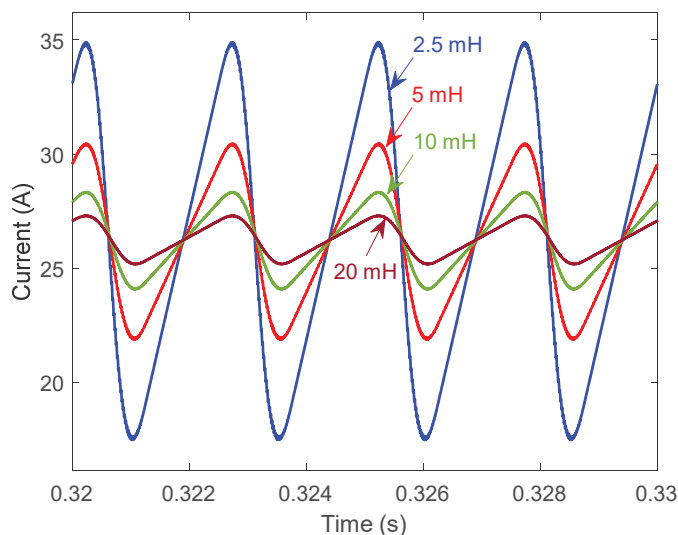


Figure 9. DC link currents as a function of various inductances.

2.2. Dynamic Load Test

Half load and double load cases are simulated using PSIM to test the inverter with the closed-loop control. For the resistive load test, a series and a parallel load are connected to the load output. Double load and half load are tested in order. 0.05 s time of operation is obtained with double and half load, respectively. In the normal load case, the obtained THD is 1.7% and the power factor (PF) is 0.98. After that double load test is performed using $20\ \Omega$. The obtained THD is 8.1% and PF is 0.98. Finally, a half load test with $5\ \Omega$

is done. 8.9% THD and almost unity PF is measured. The overvoltage and undervoltage conditions took a maximum time of 2 cycles (5 ms).

For the inductive load case, 0.8 and 0.9 PF operation modes are simulated (see Figure 10). Two series inductors (2 mH and 1 mH) are connected and activated sequentially. In the case of a purely resistive load, the obtained THD is 1.7%. After that, in the 2 mH inductive load case, a PF value of 0.9 is obtained with 1.7% THD. Finally, the 3 mH load is activated, and 0.8 PF and 1.7% THD values are acquired as expected.

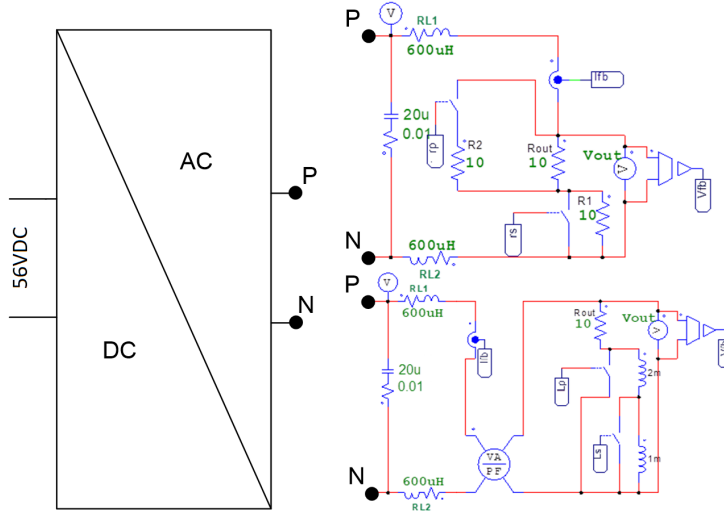


Figure 10. Simulation circuit modified for testing half and double resistive load and inductive load cases.

Figures 11 and 12 show that the control system works well for valid voltage and current outputs described in standards [10]. Furthermore, sudden changes in different loads are inspected to obtain inverter performance measurements.

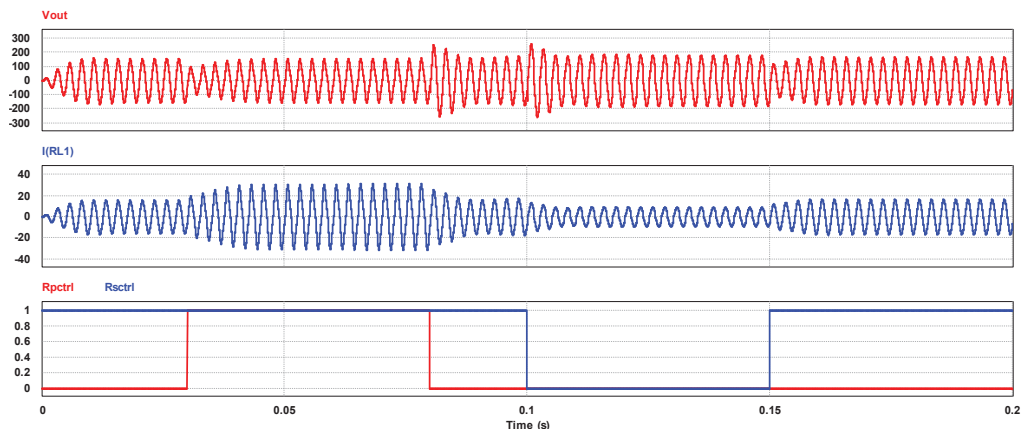


Figure 11. Simulation results for half and double load cases.

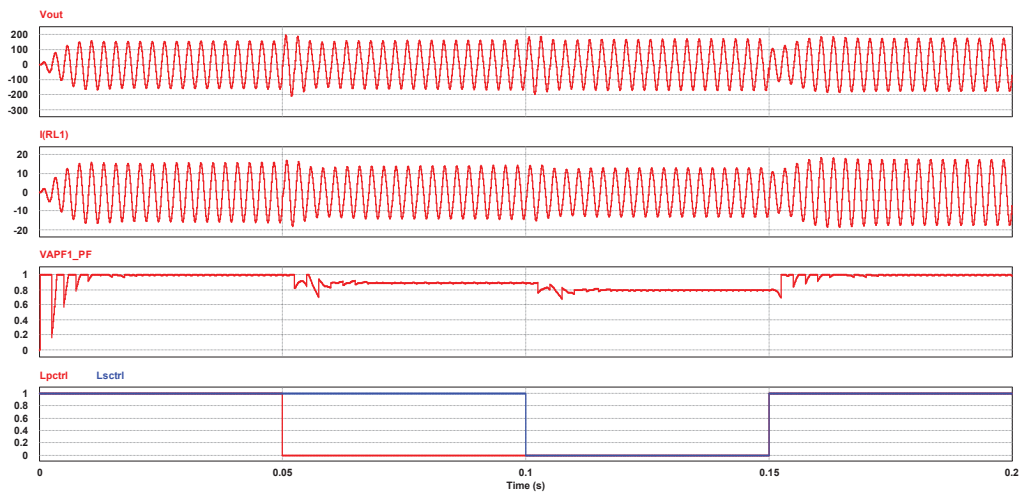


Figure 12. Simulation results for 2 mH and 3 mH load cases.

3. Experimental Results

In this work, the experimental study is done on a Typhoon HIL402 module. The characterized device can work continuously, with a 20 ns PWM goal, in a closed-loop update pace of 1 MHz with high precision for each phase of a converter framework.

Figure 13 represents the power and control stage of the designed CSI using the Schematic Editor. An embedded mixed-signal oscilloscope monitors the execution of control center test cases and performs the validation procedure with Python scripts.

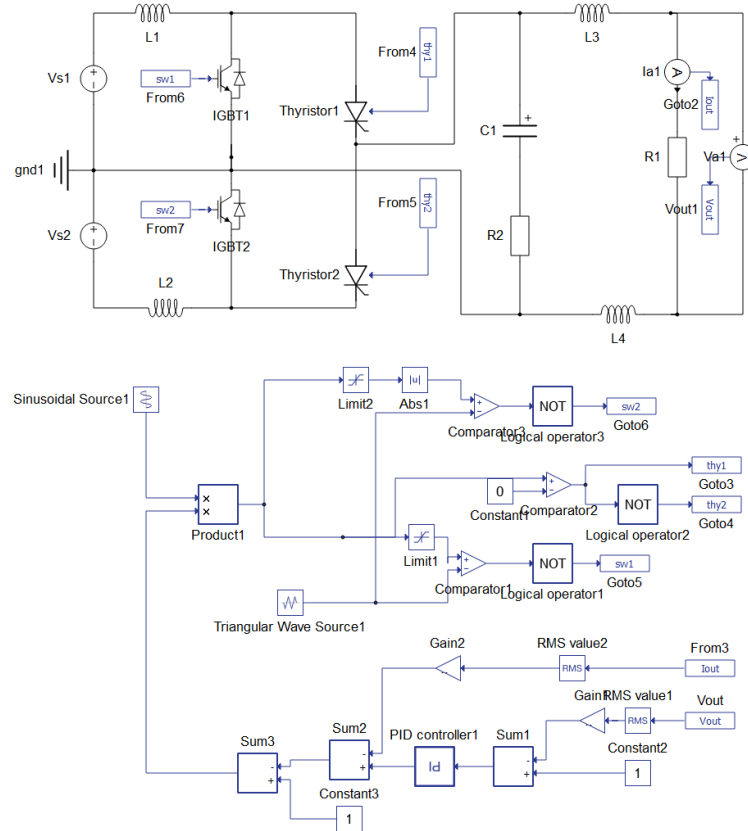


Figure 13. The proposed topology design with control using the HIL software.

As seen in Figure 13, the inverter uses two 28 V batteries (V_{S1} and V_{S2}) as input. Batteries and energy storage inductors L_1 and L_2 provide a current source input. WS switches consist of IGBTs due to some limitations of HIL. The SCR-based half-bridge inverter is used

before the low-pass filter to provide 400 Hz sinusoidal output from sinusoidally chopped DC. Line frequency pulses control the SCRs complementarily. A positive output current is produced when T_1 switch is in on state, and a negative output current is obtained when T_2 is in on state. SCR commutation is simple. The sinusoidally shaped current by the WS naturally falls below the holding current of the SCRs. A CL filter is used after the half-bridge to attenuate high-frequency PWM harmonics.

The Typhoon HIL Schematic Editor is used to design the inverter control stage. The PWM signals produced by comparing the sinusoidal waveform with the triangular waveform are sent to the IGBTs. Both are switched with complementary PWM signals. The same PWM pulses are employed for SCR switching using 'not' logic gates. As seen in Figure 14, Thyristor1 should be on when IGBT1 receives the PWM signals. The same is valid for IGBT2 and Thyristor2 sequentially. During the HIL testing, the Typhoon HIL Schematic editor uses component blocks and signal processing blocks. Typhoon HIL Scada creates PWM control signals using a PI controller. Internal modulators use an FPGA processor for high switching frequencies.

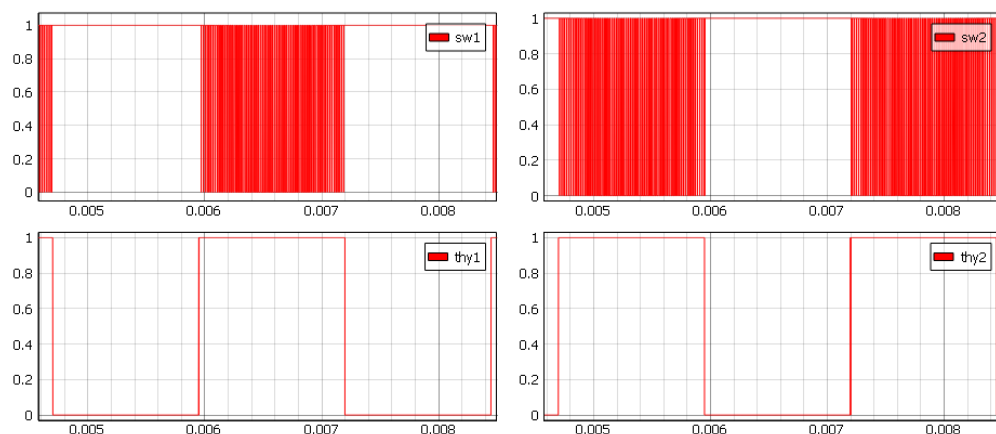


Figure 14. The WS and SCR switching signals simultaneously.

Test Procedure

The Typhoon HIL402 was used to validate the 400 Hz CSI. 50 kHz switching frequency is selected to reduce the size of the CL output filter. Please note that only SCRs have a voltage drop of 1.2 V, the rest of the CSI circuit was considered ideal while performing measurements.

Figure 15 shows the input and output waveforms of the CSI. The left waveforms are the output voltage and current using a resistive load. The waveforms in the upper right corner show the fluctuations of the DC link inductors with a frequency of 800 Hz. The ripple is high with L_1 and L_2 each having a 5 mH inductor. As seen in Figure 9 the allowable ripple current can be obtained when the inductor value has increased. The bottom right corner shows the inverter output power in Figure 15. The measured efficiency is 98% due to mainly ideal components. In current-source inverters with 50 or 60 Hz frequency output, the losses are mainly in the inductor as a fraction. Switch losses are less than the sum of core and copper losses in the inductor [32]. However, in this system, the inductor size is significantly smaller due to the 400 Hz output frequency. Thus, the bulky inductor disadvantage no longer exists. As a result, a smaller and more efficient CSI for an aircraft application is possible.

MATLAB is also used to investigate some experimental results. The model parameters of the proposed CSI are shown in Table 4. Simulations show a good agreement with experimental results.

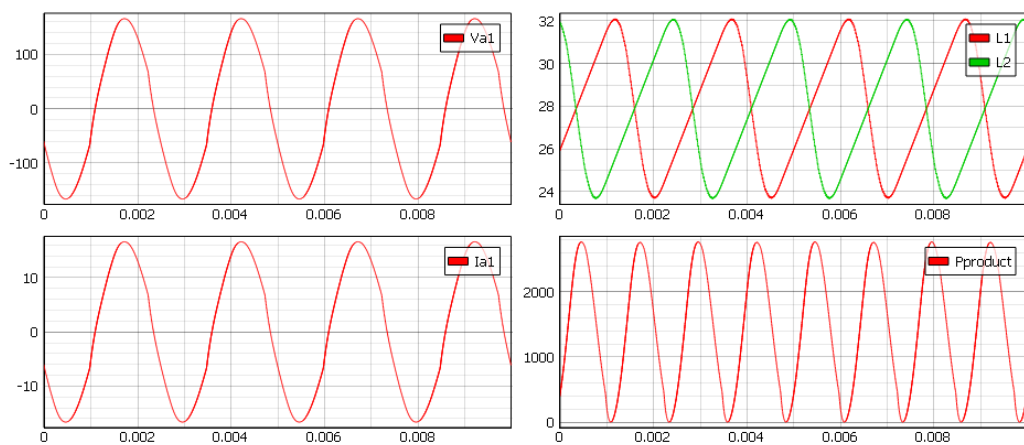


Figure 15. Proposed half-bridge inverter output waveforms are shown in Typhoon HIL SCADA. The top left corner is the output voltage (V_{a1}), the top right corner is the DC link inductor currents (L_1, L_2), the bottom left corner is the inverter output current (I_{a1}) and the bottom right corner is the output power.

Table 4. Proposed half-bridge 400 Hz CSI HIL parameters.

Parameter	Value
Output Voltage (V_{OUT})	120 V rms
Output Current (I_{OUT})	12 A rms
Output Frequency	400 Hz
Crest Factor	1.43
Output Power (P_{OUT})	1440 W
Input Power (P_{IN})	1512 W
Efficiency (%)	98
THD (%)	2.41

Figure 16 shows the FFT spectrum of the output current. In comparison to the simulated value of 1.71%, the output current total harmonic distortion is roughly 0.7% higher at 2.41%. It is possible that this is due to some assumptions made by the simulation software. Both numbers, however, are less than the maximum permissible THD value as stated in the specifications [10,31]. THD can be further reduced with control algorithm enhancements and optimized filter design.

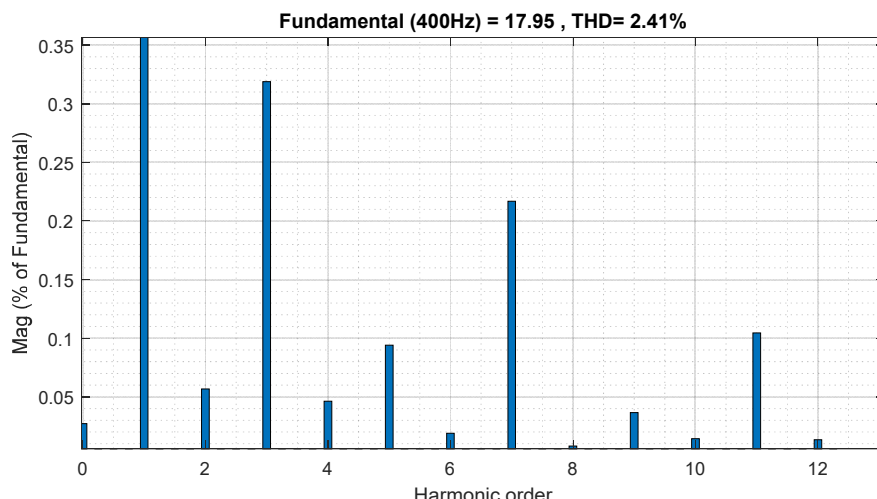


Figure 16. FFT analysis of output current.

4. Conclusions

The new single-phase half-bridge current–source inverter topology targets more electric aircraft applications mainly. Naturally, an inverter uses 400 Hz output frequency in avionics. This is a considerable advantage for current–source inverters as a significant reduction of DC link inductor size is possible. Electrolytic DC link capacitors are also omitted in CSIs.

Simulations and HIL experiments were performed and similar results were obtained. Zero current switchings occur when two high-frequency switches naturally allow commutation of thyristors without any loss. Furthermore, falling below the holding current prevents crossover distortion and contributes to keeping the THD lower. It is 2.41%, and the PF is very close to unity.

Various loads did not cause substantial changes in THD and power factor. THD and PF did not deviate from the desired values. Small DC link inductors did not reduce the inverter’s dynamic performance as it takes less time for the load current to change in response to a control command.

The proposed half-bridge CSI shows that a CSI can be smaller, lighter, and less expensive with high efficiency compared to VSIs. In addition, using fewer components in the main current path and eliminating electrolytic capacitors provides robustness and reliability. SiC or GaN semiconductors could also be used for further efficiency improvements. These features imply that the proposed CSI can be a strong candidate for aircraft applications. The CSI could be suitable for auxiliary power units, MEA, and AEA applications.

Author Contributions: Conceptualization, E.S. and G.E.; Formal analysis, E.S. and G.E.; Investigation, E.S. and G.E.; Methodology, E.S. and G.E.; Software, E.S. and G.E.; Validation, E.S. and G.E.; Writing—original draft, E.S. and G.E.; Writing—review & editing, E.S. and G.E. All authors have read and agreed to the published version of the manuscript.

Funding: This research received no external funding.

Institutional Review Board Statement: Not applicable.

Informed Consent Statement: Not applicable.

Data Availability Statement: Not applicable.

Conflicts of Interest: The authors declare no conflict of interest.

Abbreviations

The following abbreviations are used in this manuscript:

AC	Alternating current
AEA	All electric aircraft
CL	Capacitor inductor
CSI	Current–source inverter
DC	Direct current
DC/DC	Direct current to direct current converter
DC/AC	Direct current to alternating current converter (inverter)
GaN	Gallium Nitride
HIL	Hardware-in-the-loop
IGBT	Insulated-gate bipolar transistor
MEA	More electric aircraft
MOSFET	Metal oxide semiconductor field effect transistor
PF	Power factor
PWM	Pulse width modulation
rms	Root mean square
SCR	Silicon controlled rectifier (thyristor)
SiC	Silicon carbide
THD	Total harmonic distortion
VSI	Voltage-source inverter

References

1. Rosero, J.A.; Ortega, J.A.; Alabadas, E.; Romeral, L. Moving towards a more electric aircraft. *IEEE Aerosp. Electron. Syst. Mag.* **2007**, *22*, 3–9. [[CrossRef](#)]
2. Abarzadeh, M.; Kojabadi, H.M. A static ground power unit based on the improved hybrid active neutral-point-clamped converter. *IEEE Trans. Ind. Electron.* **2016**, *63*, 7792–7803. [[CrossRef](#)]
3. Mihalache, L. DSP control of 400 Hz inverters for aircraft applications. In Proceedings of the IEEE Industry Applications Conference, Pittsburgh, PA, USA, 13–18 October 2002; pp. 1564–1571.
4. Sener, E.; Ertasgin, G. Current-source 1-Ph inverter design for aircraft applications. *Aircraft Eng. Aerosp. Technol.* **2020**, *92*, 1295–1305. [[CrossRef](#)]
5. Yuan, G.; Luo, S.; Zhou, S.; Zou, X.; Zou, K. Low-order harmonics analysis and suppression method for 400 Hz single-phase VSI. In Proceedings of the IEEE Applied Power Electronics Conference and Exposition, Charlotte, NC, USA, 15–18 March 2015; pp. 2341–2345.
6. Khaligh, H.; Torkaman, H.; Ebrahimian A. Novel algorithm for optimum output passive filter design in 400 Hz inverter. In Proceedings of the IEEE Annual Power Electronics, Drives Systems and Technologies Conference, Tehran, Iran, 13–15 February 2018; pp. 335–340.
7. Jahns, T.M.; Maldonado, M.A. A new resonant link aircraft power generating system. *IEEE Trans. Aerosp. Electron. Syst.* **1993**, *29*, 206–214. [[CrossRef](#)]
8. He, J.; Zhang, D.; Torrey, D. Recent advances of power electronics applications in more electric aircrafts. In Proceedings of the AIAA/IEEE Electric Aircraft Technologies Symposium, Cincinnati, OH, USA, 12–14 July 2018; pp. 1–8.
9. Prisse, L.; Ferer, D.; Foch, H.; Lacoste, A. New power centre and power electronics sharing in aircraft. In Proceedings of the IEEE European Conference on Power Electronics and Applications, Barcelona, Spain, 8–10 September 2009; pp. 1–9.
10. MIL-STD-704F; Aircraft Electric Power Characteristics. Department of Defense Interface Standard: Washington, DC, USA, 2004.
11. Ertasgin, G.; Whaley, D.M.; Ertugrul, N.; Soong, W.L. Analysis of DC Link energy storage for single-phase grid-connected PV inverters. *Electronics* **2019**, *8*, 601. [[CrossRef](#)]
12. Yao, Z.; Wang, Z.; Blaabjerg, F.; Loh, P.C. Single-Stage Doubly Grounded Transformerless PV Grid-Connected Inverter with Boost Function. *IEEE Trans. Power Electron.* **2022**, *37*, 2237–2249. [[CrossRef](#)]
13. Alajmi, B.N.; Ahmed, K.H.; Adam, G.P.; Williams, B.W. Single-phase single-stage transformer less grid-connected PV system. *IEEE Trans. Power Electron.* **2013**, *28*, 2664–2676. [[CrossRef](#)]
14. Cai, W.; Jiang, L.; Liu, B.; Duan, S.; Zou, C. A power decoupling method based on four-switch three-port DC/DC/AC converter in DC microgrid. *IEEE Trans. Ind. Appl.* **2015**, *51*, 336–343. [[CrossRef](#)]
15. Aghaei, N.; Bizhani, H. Using fuzzy controller for improvement of power decoupling performance in PV systems. *Int. J. Electron.* **2020**, *51*, 376–389. [[CrossRef](#)]
16. Basabi, S.T.; Farzanehfard, H. Novel transistor-less series power decoupling in conventional current source inverter for PV application. In Proceedings of the IEEE Power Electronics, Drive Systems, and Technologies Conference, Iran, Tehran, 4–6 February 2020; pp. 1–5.
17. Shimizu, T.; Suzuki, S. A single-phase grid-connected inverter with power decoupling function. In Proceedings of the IEEE International Power Electronics Conference, Sapporo, Japan, 21–24 June 2010; pp. 2918–2923.
18. Hirachi, K.; Tomokuni, Y. A novel control strategy on single-phase PWM current source inverter incorporating pulse area modulation. In Proceedings of the IEEE Power Conversion Conference, Nagaoka, Japan, 3–6 August 1997; pp. 289–294.
19. Li, R.T.H.; Chung, H.S.; Chan, T.K.M. An active modulation technique for single-phase grid-connected CSI. *IEEE Trans. Power Electron.* **2007**, *22*, 1373–1382. [[CrossRef](#)]
20. Kyritsis, A.C.; Papanikolaou, N.P.; Tatakos, E.C. A novel parallel active filter for current pulsation smoothing on single stage grid-connected AC-PV modules. In Proceedings of the IEEE European Conference on Power Electronics and Applications, Aalborg, Denmark, 2–5 September 2007; pp. 1–10.
21. Zhang, J.; Ding, H.; Wang, B.; Guo, X.; Padmanaban, S. Active Power Decoupling for Current Source Converters: An Overview Scenario. *Electronics* **2019**, *8*, 197. [[CrossRef](#)]
22. Watanabe, H.; Itoh, J.I. Novel DC to single-phase AC isolated current source inverter with power decoupling capability for micro-inverter system. In Proceedings of the IEEE Energy Conversion Congress and Exposition, Aalborg, Denmark, 20–24 September 2015; pp. 158–165.
23. Lin, B.R.; Wang, K.W. Interleaved soft switching resonant converter with a small input ripple current. *Int. J. Electron.* **2020**, *107*, 644–658. [[CrossRef](#)]
24. Tarter, R.E. Current-fed converters. In *Solid-State Power Conversion Handbook*, 1st ed.; Wiley-Interscience: New York, NY, USA, 1993; pp. 429–433.
25. Madonna, V.; Migliazza, G.; Giangrande, P.; Lorenzani, E.; Buticchi, G.; Galea, M. The rebirth of the current source inverter: advantages for aerospace motor design. *IEEE Ind. Electron. Mag.* **2019**, *13*, 65–76. [[CrossRef](#)]
26. Mazda, F. The current-fed inverter. In *Power Electronics Handbook*, 3rd ed.; Newnes: Oxford, UK, 1997; pp. 345–350.
27. Xiong, Y.; Oyane, A.; Ou, T.; Thilak, S.; Imaoka, J.; Yamamoto, M. Comparison of switching performance between GaN and SiC MOSFET via 13.56 MHz Half-bridge Inverter. In Proceedings of the IEEE International Symposium on Industrial Electronics, Delft, The Netherlands, 17–19 June 2020, pp. 672–676.

28. Kamli, M.; Yamamoto, S.; Abe, M. A 50–150 kHz half-bridge inverter for induction heating applications. *IEEE Trans. Ind. Electron.* **1996**, *43*, 163–172. [[CrossRef](#)]
29. Wang, X.; Loh, P.C.; Blaabjerg, F. Stability analysis and controller synthesis for single-loop voltage-controlled VSIs. *IEEE Trans. Power Electron.* **2017**, *32*, 7394–7404. [[CrossRef](#)]
30. Wang, X.; Li, Y.W.; Blaabjerg, F.; Loh, P.C. Virtual-impedance - based control for voltage-source and current-source converters. *AIEEE Trans. Power Electron.* **2015**, *30*, 7019–7037. [[CrossRef](#)]
31. IEEE Standard 519-2014; IEEE Recommended Practice and Requirements for Harmonic Control in Electric Power Systems. IEEE-SA Standards Board: Piscataway, NJ, USA, 2014.
32. Ertasgin, G.; Soong, W.L.; Ertugrul, N. Analysis and design of single-phase current-source grid-connected PV inverter. In Proceedings of the IEEE European Conference on Power Electronics and Applications, Lille, France, 2–6 September 2013; pp. 1–10.